COVID-19 IMAGE CLASSIFICATION OF POSITIVE AND NEGATIVE PATIENTS FROM X-RAY IMAGES USING DEEP LEARNING

Suyog Nemade

Student Dept. of Information Technology Engineering, Shah & Anchor Kutchhi Engineering College, Mumbai, India

---

Abstract - *The global epidemic of COVID-19 has wreaked havoc on all aspects of our lives. A lot in particular, health care systems were highly expanded to their limits and beyond. Progress in The installation ingenuity has allowed the implementation of complex applications that may be met clinical accuracy requirements. In this study, in-depth and pre-trained study models were based on convolutional neural networks used to detect pneumonia caused by COVID-19 respiratory problems. Chest X-ray images from 370 patients confirmed COVID-19 patients were collected locally. In addition, data from three public data sets was used. Performance tested on four ways. First, the public database was used for training and testing. Second, location information and community resources were mobilized and used to train and test models. Third, the public database was used for model training and local data was used for testing only. This method adds more loyalty to acquisition models also tests their ability to create new information without over-discovery model in certain samples. Fourth, aggregated data was used for training and local databases was used for testing. The results show a high acquisition accuracy of 98.7% with aggregated data, and many models handle new details with an insignificant decrease in clarity.*

Key Words: COVID-19; chest X-ray; deep learning; convolutional neural networks; diagnosis

1. INTRODUCTION

Coronavirus 2019 (COVID-19), caused by the SARS-CoV-2 virus, has severely damaged humanity, especially health systems. Recently, for example, a wave of infections in India has caused many families to seek home care due to a shortage of critically ill units. Millions worldwide have been affected by the epidemic, and many more have suffered from chronic and short-term health problems[1]. The most common symptoms of the virus are fever, dry cough, fatigue, aches and pains, loss of taste / smell, and respiratory problems. Other very rare symptoms may occur (e.g., diarrhea, conjunctivitis)[2]. Infection is officially confirmed using a real-time reverse transcription polymerase chain reaction (RT-PCR)[3]. However, chest radiographs using chest chest X-ray (CXRs) and computerized tomography (CT) play an important role in confirming infection and assessing the extent of damage to the lungs. CXR and CT scans are considered to be the main evidence for the clinical diagnosis of COVID-19[4].

Chest X-ray images are one of the most common diagnostic techniques in the clinic. However, reaching the right conclusion requires special knowledge and experience. Pressure on medical personnel worldwide caused by the COVID-19 epidemic, in addition to existing an insufficient number of radiologists for individual individuals worldwide[5], requires new and accessible solutions. Advances in artificial intelligence have led to the use of sophisticated applications that can meet the requirements of clinical accuracy and capture large amounts of data. Installing computer-assisted diagnostic tools in the medical field has the potential to reduce errors, improve workload conditions, increase reliability, and instead improve workflow and reduce diagnostic errors by providing radiologists with diagnostic guidelines.

The war against COVID-19 has taken several forms and stages. Computerized solutions provide alternative means of communication in many aspects of dealing with the epidemic[6.] Other examples include robots for physical sampling solutions, monitoring key signals ,and disinfection. In addition, image recognition and AI are actively used to identify verified cases that do not follow incarceration agreements. In this work, we propose an automatic artificial intelligence (AI) screening program that can detect COVID-19-related pneumonia in chest X-ray images with high accuracy. One convolutional neural networks model and two previously trained models (namely, MobileNets[7] and VGG16[8]) were included. In addition, CXR images of COVID-19 certified subjects were collected at an area major hospital and evaluated by board-approved specialists in time. 6 months. These images have been used to enrich a limited number of public data sets and to form a large group of training / testing of images compared to related books. Importantly, the reported results came from testing the models with this set of external images completely in addition to testing the models using an aggregate set. This approach has exposed any model overlap in a particular set of CXR images, especially since some data sets contain multiple images per subject.

2. Background and Related Work

COVID-19 patients with clinical symptoms may show abnormal CXR[9]. Key findings in a recent study suggest that these lung images show reticular-nodular abnormalities and connective tissue, and basal, peripheral, and dual domination[10]. For example, Figure 1 shows the CXR of alittle case of lung tissue involvement with appropriate infrahilar reticular-nodular opacity. In addition, Figure 2 shows the CXR of the moderate to severe case of lung tissue involvement. This is CXR shows the fusion of the lungs in the lower right and separates the two reticular – nodular

airspace opacities, most prominent in the surrounding areas of low-lying areas. Similarly, Figure 3 shows the CXR of the severe case of lung tissue involvement. This is due to the airspace variations on both sides of the reticular – nodular opacities that are most noticeable in the lateral parts of the lower extremities, and the diminution of the lower glass in both lungs that are prominent in the central and lower extremities. On the other hand, Figure 4 shows an unparalleled CXR with clear lungs and acute costophrenic angles (i.e., normal).

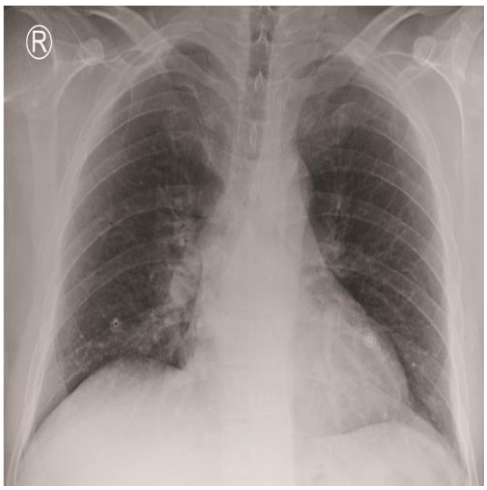

Figure 1. CXR of COVID-19 subject showing mild lung tissue involvement.

Figure 2. CXR of COVID-19 subject showing moderate to severe lung tissue involvement.

Figure 3. CXR of COVID-19 subject showing severe lung tissue involvement

Figure 4. Normal CXR.

AI, with its basic machine learning (ML), has taken a major step in application in many fields. For example, Vetology AI[11] is a paid AI service that provides AI-based radiograph reports. Similarly, widespread research and the use of AI in medicine have been around for years[12,13]. AI-based web or automated diagnostic mobile applications can greatly assist physicians in reducing errors, providing long and cheap diagnoses in poor and poor facilities, and improving speed and quality. of health care[14]. In the context of COVID-19 radiographs, ML methods can detect CXR images to detect the above-mentioned symptoms of COVID-19 infection and adverse effects on patients' lungs. This is especially important when considering the fact that health services expanded to their limits and sometimes reached the brink of collapse from the epidemic.

Deep learning AI enables the development of end-to-end models that learn and acquire classification patterns and features using multiple layers of processing, providing unnecessary to exclude features obviously. The sudden spread of the COVID-19 epidemic has necessitated the development of new approaches to address the growing health care needs of these outbreaks. To date, many recent

models have been proposed for the discovery of COVID19. These methods rely heavily on CXR and CT imaging as inclusion in the diagnostic model[15,16]. Hemdan et al.[17] proposed a comprehensive study framework for COVIDX-Net to classify CXR images as positive or negative for COVID-19. Although they used seven convolutional neural network models, the best results were 89% and 91% of F1 effects of normal and positive COVID-19, respectively. However, their results were based on 50 CXR images only, which is a very small database for building reliable depth learning program.

Several existing out-of-the-box in-depth convolutional neural network algorithms are available in the literature[18], and are widely used in COVID-19 diagnostic literature without modification[15]. They provide proven image detection and diagnostic skills in many fields and research problems. Some of the foremost widely used models are: (1) GoogleNet, VGG-16, VGG-19, AlexNet, and LetNet, which are CNNs supported location exploitation. (2) MobileNet, ResNet, InceptionV3, and Inception-V4, which are deep-based CNNs. (3) Other models contain DenseNet, Xception, SqueezeNet, etc. These structures can be used in advance training for in-depth transfer learning (e.g., Sethy et al.[19]), Or customized (e.g., CoroNet[20]).

Rajaraman et al.[21] Extensively cut-out reading ensembles were used to differentiate CXRs from standard, COVID-19, or bacterial pneumonia with 99.01% accuracy. Several models were tested and the best results were combined using a variety of blending techniques to improve the accuracy of the sections. However, such methods are particularly suitable for small numbers of COVID-19 images as the statistical value of most models is high, and there is no guarantee that they will maintain their accuracy with large databases[22]. Some of the functions of the division into three categories using in-depth study were and proposed in this context. Studies by Ucar et al.[23] , Rahimzade and Attar[24], Narin et al.[25] , and Kobahi et al.[26] classify cases such as COVID-19, common, or pneumonia. Some switch to pneumonia into a category that is not generic COVID-19[27,28], or acute acute respiratory syndrome (SARS). Gradually, the study distinguishes between viral and bacterial pneumonia in four stages. A significant number of studies have made two divisions into COVID-19 or non-COVID-19 classes[30]. Although these methods have achieved high accuracy (i.e., over 89%), the number of COVID-19 images from the database is small. For example, Ucar et al.[23] used only 45 COVID-19 images. In addition, subsequent testing of models used a subset of the same database, which could provide false enhanced results, especially since the same subject may have multiple CXR images in the database.

3. Material and Methods

3.1. Subjects

Selected images were obtained from chest X-rays recorded on the site of COVID-19 patients in addition to publicly available data[31]. The combination of the two databases adds great reliability to advanced diagnostic models. This is because the training / certification is done on one set, and the tests are done on a different database. In addition, it has increased the size of the database, which is a problem with many related books.

The first group of photographs were found at King Abdullah University Hospital, Jordan University of Science and Technology, Irbid, Jordan. The study was commissioned by the institutional review board (IRB 91/136/2020) at King Abdullah University Hospital (KAUH). Informed written consent was sought and obtained from all participants (or their parents in case they were under age) prior to any clinical trials. The database included 368 subjects (215 males, 153 females) aged ± SD of 63.15 ± 14.8. The minimum academic age was 31 months and the maximum age was 96. All subjects had at least one RT-PCR test and required hospitalization as determined by experts at KAUH. Staying in the hospital ranged from 5 days to 6 weeks with some subjects passing away (exact number not available). CXR images were taken after at least 3 days in the hospital to confirm that there was something wrong with the lungs, which was present confirmed by participating professionals. CXR images were updated using the MicroDicom viewerversion3.8.1(seehttps://www.microdicom.com/, accessed: 28 May 2021), and shipped as high-resolution images (i.e., pixels 1850 × 1300).

The second group of images is publicly available[31], and was produced by a combination of three different databases: (1) COVID-19 chest X-ray dataset[32]. (2) Data set for the Radiological Society of North America (RSNA)[33]. (3) U.S. X-ray set National Library of Medicine (USNLM) Montgomery County X-ray[34]. At the time of the experiment, the data set contained 2295 CXR images (1583 standard and 712 COVID-19), which were used for this task. However, the data set is updated continuously[35].

3.2. Deep Learning Models

Deep learning is a current practice and most used AI methods used for classification problems. It has been widely used and successfully in a variety of applications, especially in the medical field. The next few sections describe the models used in this work.

1. 2D consecutive CNN models are one class in in-depth textbooks. They are a special class of neural networks that are found to be very useful in analyzing multidimensional data (e.g., images) . However, CNN preserves memory related to multi-layer ideas by sharing parameters and using fewer connections. Input images are converted into a matrix that will be processed by various CNN features. The model contains a few alternating layers of flexibility and integration (see Table 1), as follows:

Convolutional layer
The convolution layer determines the features of the various patterns in the input. It contains a set of dot products (i.e., convolutions) used in the input matrix. This step creates an image processing kernel that contains a number of filters, which produce a feature map (i.e., motifs). Input is divided into small windows called reception fields, which are integrated with the kernel using a specific set of weights. In this work, a 2D layer of conviction (i.e., using the CONV2D phase) is used).

Pooling layer
This down sample layer reduces the size of the output volume area reduce the number of feature maps and network parameters. In addition, integration helps to improve the overall performance of the model by reducing overlap[36]. I the output in this step is a combination of fixed elements in translation and distortion shifts[37].

Dropout
Overuse is a common problem in neural networks. Therefore, dropout is used as a
a strategy to introduce familiarity within the network, which ultimately improves normal performance. It works randomly by ignoring other hidden and visible units. This has the effect of training the network to handle many independent internal presentations.

Fully connected layer
This layer accepts the feature map as an insert and removes indirect modified output with the activation function. This is a global function that works on elements from all categories to produce an indirect set of distinctive features. The modified line unit (ReLU) was used in this step as it helps to overcome the problem of perishable gradient[38].

Table 1. Summary of the CNN models used in this work.

Summary of the CNN models used in this work.		
Layer	**Output Shape**	**No. of Parameters**
CONV2D-1	(None, 150, 150, 32)	2432
MaxPooling2D-1	(None, 75, 75, 32)	0
Dropout-1	(None, 75, 75, 32)	0
Conv2D-2	(None, 75, 75, 64)	51,264
MaxPooling2D-2	(None, 37, 37, 64)	0
Dropout-2	(None, 37, 37, 64)	0
Flatten	(None, 87,616)	0
Dense-1	(None, 256)	22,429,952
Dropout-3	(None, 256)	0
Dense-2	(None, 1)	257

2. Pre-trained models
MobileNets
The MobileNets model is a CNN-based software platform, selected for this purpose based on the mobile application of the future diagnosis. It uses highly differentiated convolutions, which greatly reduces the number of parameters. MobileNets has been provided with open source by Google to enable the development of low power, small applications, and minimal mobile applications.

VGG-16
VGG-16 represents many of the existing models in the literature. It has undergone various improvements to improve its efficiency and use of resources (e.g., VGG-19). The VGG model is a 19-layer CNN site exploitation, 3 × 3 filters (computerized), 1 × 1 flexibility between layers of convolution (regular), and high consolidation after the convolution layer. The model is known for its simplicity

3.3 Model Implementation

Models are used and tested using the TensorFlow Keras[39] (API) application TensorFlow2[40]. Tested on Dell Precision 5820 Tower with Intel Xeon W-2155, 64GB RAM and 16GB Nvidia Quadro RTX5000 GPU.

4.Results and Discussion

Four different methods were used to test the three in-depth study models. First, only the public database was used to train and evaluate the models. Second, integrated data was used to evaluate and train models (i.e., sets are grouped together and treated as one without any differences). Third, the public database was used for model training and the local data collected was used for testing. This approach demonstrates competence model to integrate new data and avoid overcrowding in certain images / subjects. Fourth, aggregated data (i.e., aggregated) was used for training and a set of local data for testing. Table 2 show the number of training and assessment courses used for each method. Note that the local database did not include standard CXR images as those are available in bulk. The matrices of confusion due to testing are analyzed to produce a few common performance measures. These include accuracy, precision, sensitivity, F1 effect, and accuracy as defined in Standards (1) - (5)

Table 2. The number of training and testing subjects used for each of the evaluation approaches.

The number of training and testing subjects used for each of the evaluation approaches.				
Approach	Training		Testing	
	COVID-19	Normal	COVID-19	Normal
Public dataset	545	1266	167	317
Fused dataset	842	1266	238	317

Public dataset for training and local dataset for testing	545	1266	368	317
Fused dataset for training and local dataset for testing	842	1266	368	317

$$Accuracy = \frac{tp + tn}{tp + fn + fp + tn} \quad (1)$$

$$Sensitivity = \frac{tp}{tp + fn} \quad (2)$$

$$Specificity = \frac{tn}{tn + fp} \quad (3)$$

$$F1score = \frac{2 \times tp}{2 \times tp + fp + fn} \quad (4)$$

$$Precision = \frac{tp}{tp + fp} \quad (5)$$

where tp: true positive, stands for pre-arranged studies (positive) class.
fn: false negative, represents subjects that are not well classified in another category (negative).
fp: false positive, representing subjects that are not well classified in the pre-defined (good) category.
tn: Real negative, represents well-organized lessons in another (negative) category.

Figure 5 shows the loss of training and validation of the two model training methods. The CND 2D model needed more time to achieve the correct accuracy development, but the training was smooth and with minimal oscillation. In addition, the other two models required very few sessions (e.g., VGG-16 required one period and the combined data, hence the plan is not available). Figure 6 shows the accuracy of training and certification. Statistics often show that the models are able to fine-tune the training data and improve with knowledge. It is clear that the MobileNets and VGG-16 models achieve higher and higher stage accuracy. The test database (i.e., COVID-19 CXR images collected locally) is different from the training database

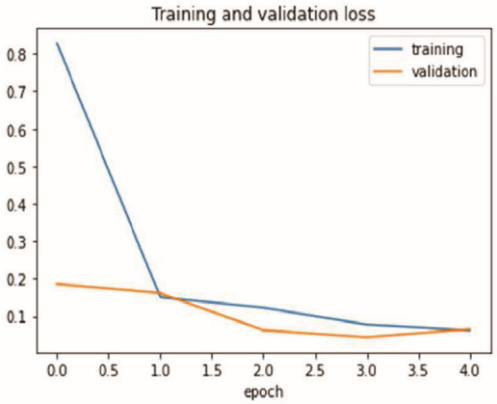

(a) CNN trained using the public dataset.

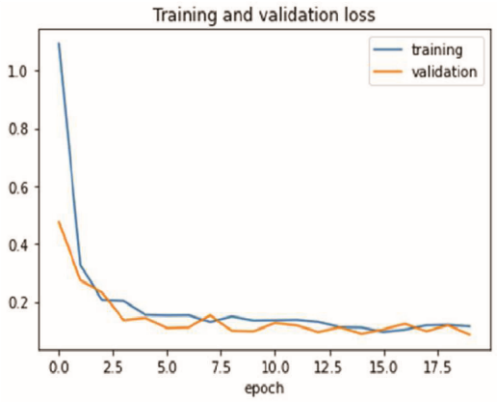

(**b**) CNN trained using the fused dataset.

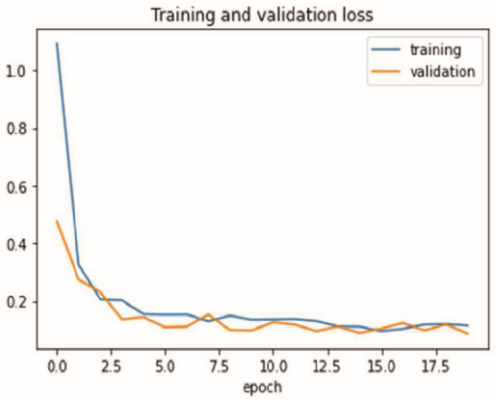

(**c**) MobileNets trained using the public dataset

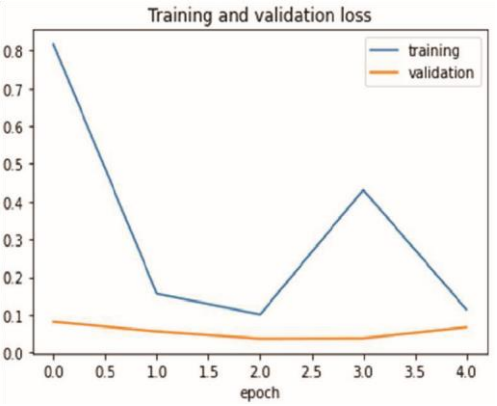

(**d**) MobileNets trained using the fused dataset.

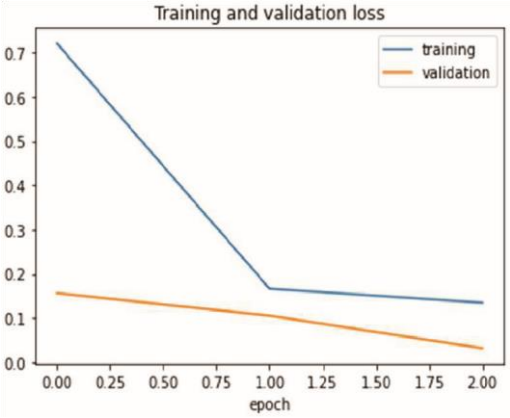

(**e**) VGG-16 trained using the public dataset.

Figure 5

Figure 5. Training and loss of validation of three community-trained facilities with integrated databases. Note that VGG-16 integrated datasets expire after only one period, so there is no corresponding value. Models are able to fine-tune training data and improve knowledge (as evidenced by validation curves).

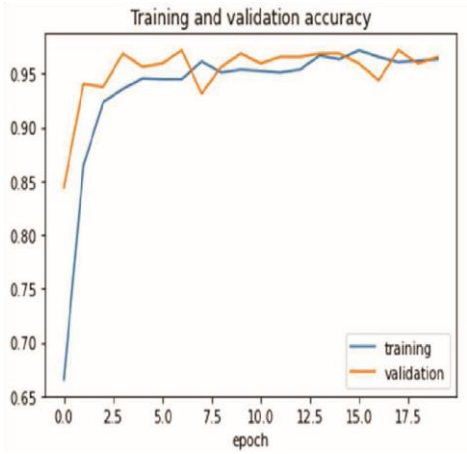

(**a**) CNN trained using the public dataset.

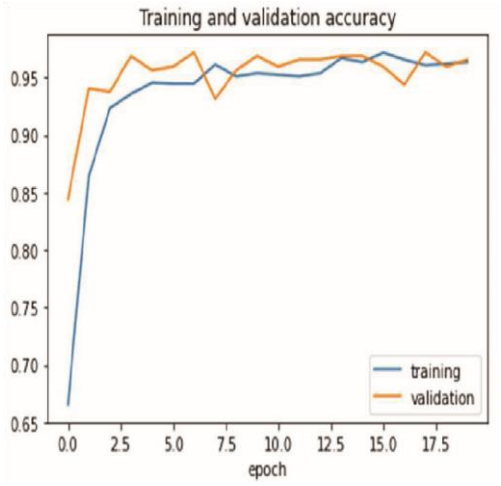

(**b**) CNN trained using the fused dataset.

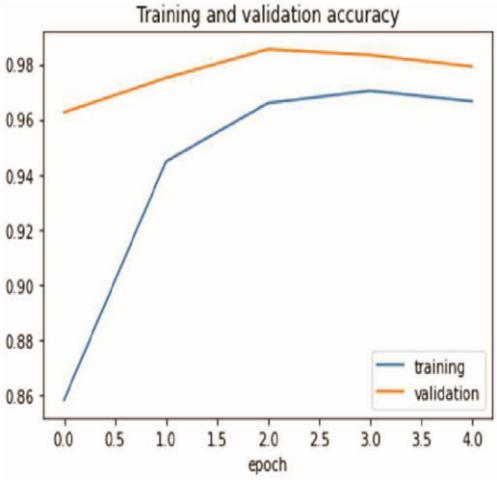

(**c**) MobileNets trained using the public dataset.

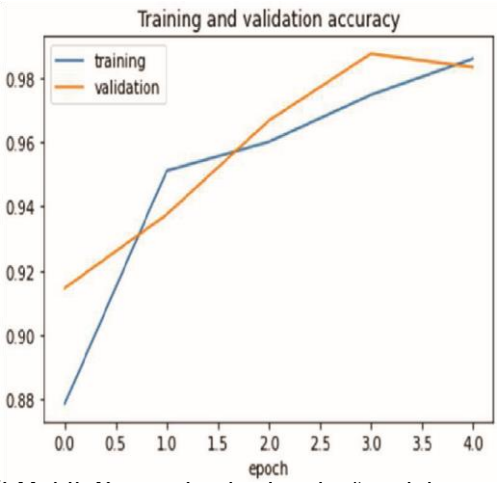

(**d**) MobileNets trained using the fused dataset.

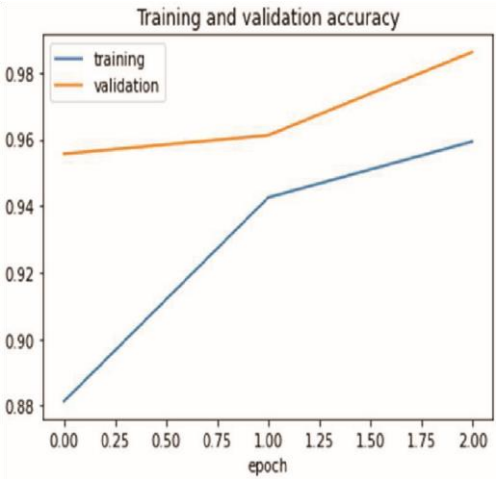

(**e**) VGG-16 trained using the public dataset.

Figure 6.

Figure 6. Training and verification of the accuracy of three community-trained facilities and integrated data sets. Note that VGG-16 integrated datasets expire after only one period, so there is no corresponding value. Models are able to fine-tune training data and improve knowledge (as evidenced by validation curves).

4.1. 2D Sequential CNN

Tables 3 and 4 show the metrics for performance analysis and parallel confusing matrices of CNN 2D sequential 2D model. Architecture achieved the best 96.1% accuracy in all training methods and testing methods. However, the accuracy decreases significantly to 79% when tests are performed using a site (i.e., COVID-19 CXR images collected locally) that are different from training (i.e., set of public data). This indicates a model failure to integrate new data, and that there may be subtle or obscure differences between images from two data sets. This is further confirmed by the fact that standard images (see Table 4c), taken from public databases, are generally classified accordingly. The source of the errors is derived from the false negative classification (i.e., type II errors). However, the accuracy has improved to 88%, when a different portion of the test database was included in the training. However, most errors were type II (see Table 4d). This is a problem of variability in the performance of the CNN custom model, often caused by unsupported data samples. However, as other models are trained with the same data, this reason may be reduced. MobileNets and VGG-16 models are employed using transfer learning, which naturally reduces overload. In addition, these models are larger and deeper than the custom CNN, which due to the parameters of the parameter can lead to normal operation.

Table 3. Performance evaluation metrics for the customized CNN model. Acc.: Accuracy, Sens.: Sensitivity, Spec.: Specificity, Prec.: Precision.

Performance evaluation metrics for the customized CNN model.					
Dataset	**Acc.**	**Sens.**	**Spec.**	**F1-Score**	**Prec.**
Public dataset	96.1%	92.8%	97.8%	94.2%	95.7%
Fused dataset	93.7%	85.7%	99.7%	92.1%	99.5%
Public dataset for training and local dataset for testing	79%	62.8%	97.8%	76.2%	97.1%
Fused dataset for training and local dataset for testing	88%	80.4%	99.7%	89%	99.7%

Table 4. The confusion matrices resulting from the customized CNN model. Positive refers to confirmed COVID-19 case

a) Public Dataset			
		Predicted diagnosis	
		Positive	Negative
Actual	Positive	155	12
	Negative	7	310
(b) Fused Public and Local Datasets			
		Predicted diagnosis	
		Positive	Negative
Actual	Positive	204	34
	Negative	1	316
(c) Public Dataset for Training and Local Dataset for Testing			
		Predicted diagnosis	
		Positive	Negative
Actual	Positive	231	137
	Negative	7	310
(d) Fused Dataset for Training and Local Dataset for Testing			
		Predicted diagnosis	
		Positive	Negative
Actual	Positive	296	72
	Negative	1	316

4.2. MobileNets

Tables 5 and 6 show the metrics for performance measurement and compatible confusion matrics for MobileNets model. It found accuracy rates between 97.1% and 98.7%, indicating stability in the face of new data, and the ability to integrate. Errors, though few, were created to classify COVID-19 CXR images as normal. However, errors of type I increased slightly (Table 6c).

Table 5. Performance evaluation metrics for the customized MobileNets model. Acc.: Accuracy, Sens.: Sensitivity, Spec.: Specificity, Prec.: Precision.

Performance evaluation metrics for the customized MobileNets model.					
Dataset	**Acc.**	**Sens.**	**Spec.**	**F1-Score**	**Prec.**
Public dataset	98.3%	98.2%	98.4%	97.6%	97%
Fused dataset	97.1%	92.8%	99.4%	95.7%	98.7%
Public dataset for training and local dataset for testing	98%	97.6%	98.4%	98.1%	98.6%
Fused	98.7%	98.1%	99.4%	98.8%	99.4%

dataset for training and local dataset for testing					

Table 6. The confusion matrices resulting from the customized MobileNets model. Positive refers to confirmed COVID-19 case.

a) Public Dataset			
		Predicted diagnosis	
		Positive	Negative
Actual	Positive	164	3
	Negative	5	312
(b) Fused Public and Local Datasets			
		Predicted diagnosis	
		Positive	Negative
Actual	Positive	155	12
	Negative	2	315
(c) Public Dataset for Training and Local Dataset for Testing			
		Predicted diagnosis	
		Positive	Negative
Actual	Positive	359	9
	Negative	5	312
(d) Fused Dataset for Training and Local Dataset for Testing			
		Predicted diagnosis	
		Positive	Negative
Actual	Positive	361	7
	Negative	2	315

4.3. VGG-16

Tables 7 and 8 show the metrics for performance measurement and compatible confusion matrics for VGG-16 model. The model obtained the best accuracy of all models (i.e., 99%) where the combined database is used for training and the local database is used for testing, which demonstrates its ability to capture different properties in different sets. However, it fell behind MobileNets slightly when the training database (i.e., the public database) differed from the test database. In addition, the model obtained very high accuracy (98.7%) with your combined database for both training and testing. However, MobileNets has gained a bit of a higher accuracy when it is trained and tested by the public database alone. Such a small difference in performance when the database is supplemented with data from other sources may require further investigation. Confused matriculants indicate that, in VGG-16, most errors are type I in all test methods, as opposed to errors in CNN or MobileNets (i.e., type II). Improving VGG-16 management of standard images should reduce the level of errors significantly.

Table 7. Performance evaluation metrics for the customized VGG-16 model. Acc.: Accuracy, Sens.: Sensitivity, Spec.: Specificity, Prec.: Precision.

Performance evaluation metrics for the customized VGG-16 model.					
Dataset	**Acc.**	**Sens.**	**Spec.**	**F1-Score**	**Prec.**
Public dataset	97.1%	98.2%	96.5%	95.9%	93.7%
Fused dataset	98.7%	99.2%	98.4%	98.5%	97.9%
Public dataset for training and local dataset for testing	97.2%	97.8%	96.5%	97.4%	97%
Fused dataset for training and local dataset for testing	99%	99.5%	98.4%	99.1%	98.7%

Table 8. The confusion matrices resulting from the customized VGG-16 model. Positive refers to confirmed COVID-19 case.

a) Public Dataset			
		Predicted diagnosis	
		Positive	Negative
Actual	Positive	164	3
	Negative	11	306
(b) Fused Public and Local Datasets			
		Predicted diagnosis	
		Positive	Negative
Actual	Positive	236	2
	Negative	5	312
(c) Public Dataset for Training and Local Dataset for Testing			
		Predicted diagnosis	
		Positive	Negative
Actual	Positive	360	8
	Negative	11	306
(d) Fused Dataset for Training and Local Dataset for Testing			
		Predicted diagnosis	
		Positive	Negative
Actual	Positive	366	2
	Negative	5	312

4.4. Comparison to Related Work

Table 9 shows the performance comparisons of deep learning lessons in binary classification using CXR images. Some studies did not report accuracy as their data sets were unequal. Although many related studies have reported high levels of accuracy, a common theme among them is the lack of a significant number of COVID-19 cases of this type of separation model. For example, Narin-et-al. state that an excessive number of standard images caused high accuracy in all those models. This is vanity considering the fact that there is very little difference between the normal lung images in different subjects. Similarly, Hemdan et al. identified a limited number of COVID-19 X-ray images as a major problem in their work. In addition, the database that we have included in this project contains only one image per subject, unlike other data sets that include more images than topics. In addition, the type of cases included in the database was specifically considered, because the effect of COVID-19 on the lungs is not really pronounced. appear immediately with symptoms and may take a few days. In deep learning textbooks for general medical diagnosis and COVID-19 the division is especially large and growing. However, large data sets are needed to have standard and reliable models. We believe that the development of more accessible and accessible mobile apps that capture and store data faster will allow for better data collection and in-depth learning models developed

Table 9. Performance comparison of deep learning studies in binary COVID-19 diagnosis (i.e., positive or negative) using CXR images. Some studies did not report the accuracy as their datasets were largely imbalanced. All websites were last accessed on 28 May 2021.

Study	Method	Accuracy
Singh et al. [42]	MADE-based CNN	94.7%
Sahinbas et al. [43]	VGG16, VGG19, ResNet, DenseNet, InceptionV3	80%
Medhi et al. [44]	Deep CNN	93%
Narin et al. [25]	InceptionV3, ResNet50, ResNet101	96.1%
Sethy et al. [19]	most available models (e.g., DenseNet, ResNet)	95.3%
Minaee et al. [30]	ResNet18, ResNet50, SqueezeNet, DenseNet-121	–
Maguolo et al.[45]	AlexNet	–
Hemdan et al. [17]	VGG19, ResNet, DenseNet, Inception, Xception	90%
This work	2D CNN, VGG16, MobileNets	up to 99%

5. Conclusions

Global disasters bring people together and inspire new things. The current epidemic and the devastating effects of globalization should present an opportunity to advance technological solutions that help in everyday life. In this study, we collected X-ray images of patients from hospitalized COVID-19. This data will enrich the existing public data sets and enable additional configurations for the systems they use. In addition, intelligent models for in-depth learning activities are designed, trained, and evaluated using locally collected databases and public data sets, both separately and integrated. The results of high accuracy provide an opportunity to improve portable and simple applications that improve diagnostic accuracy, reduce the burden on struggling health workers, and provide better access to health care in poorly maintained / poor facilities. Future work will focus on this approach as well as the development and testing of models divided into multiple categories.

References

1. Huang, C.; Wang, Y.; Li, X.; Ren, L.; Zhao, J.; Hu, Y.; Zhang, L.; Fan, G.; Xu, J.; Gu, X.; et al. Clinical features of patients infected with 2019 novel coronavirus in Wuhan, China. Lancet **2020**, 395, 497–506. [CrossRef]
2. CDC. Symptoms of COVID-19. 2021. Available online: https://www.cdc.gov/coronavirus/2019-ncov/symptoms-testing/ symptoms.html (accessed on 25 May 2021).
3. Axell-House, D.B.; Lavingia, R.; Rafferty, M.; Clark, E.; Amirian, E.S.; Chiao, E.Y. The estimation of diagnostic accuracy of tests for COVID-19: A scoping review. J. Infect. **2020**, 81, 681–697. [CrossRef]
4. Zu, Z.Y.; Jiang, M.D.; Xu, P.P.; Chen, W.; Ni, Q.Q.; Lu, G.M.; Zhang, L.J. Coronavirus Disease 2019 (COVID-19): A Perspective from China. Radiology **2020**, 296, E15–E25. [CrossRef]
5. WHO. Medical Doctors (per 10 000 Population). 2021. Available online: https://www.who.int/data/gho/data/indicators/ indicator-details/GHO/medical-doctors-(per-10-000-population) (accessed on 28 May 2021).
6. Khamis, A.; Meng, J.; Wang, J.; Azar, A.T.; Prestes, E.; Li, H.; Hameed, I.A.; Takács, Á.; Rudas, I.J.; Haidegger, T. Robotics and Intelligent Systems Against a Pandemic. Acta Polytech. Hung. **2021**, 18, 13–35. [CrossRef]
7. Howard, A.G.; Zhu, M.; Chen, B.; Kalenichenko, D.; Wang, W.; Weyand, T.; Andreetto, M.; Adam, H. MobileNets: Efficient Convolutional Neural Networks for Mobile Vision Applications. arXiv **2017**, arXiv:1704.04861.
8. Simonyan, K.; Zisserman, A. Very Deep Convolutional Networks for Large-Scale Image Recognition. In

Proceedings of the 3rd International Conference on Learning Representations, ICLR 2015, San Diego, CA, USA, 7–9 May 2015.

9. Samrah, S.M.; Al-Mistarehi, A.H.W.; Ibnian, A.M.; Raffee, L.A.; Momany, S.M.; Al-Ali, M.; Hayajneh, W.A.; Yusef, D.H.; Awad, S.M.; Khassawneh, B.Y. COVID-19 outbreak in Jordan: Epidemiological features, clinical characteristics, and laboratory findings. Ann. Med. Surg. **2020**, 57, 103–108. [CrossRef] [PubMed]

10. Cozzi, D.; Albanesi, M.; Cavigli, E.; Moroni, C.; Bindi, A.; Luvarà, S.; Lucarini, S.; Busoni, S.; Mazzoni, L.N.; Miele, V. Chest X-ray in new Coronavirus Disease 2019 (COVID-19) infection: findings and correlation with clinical outcome. La Radiol. Med. **2020**, 125, 730–737. [CrossRef] [PubMed]

11. AI Vetology. AI Vetology. 2021. Available online: https://vetology.ai/ (accessed on 25 May 2021).

12. Greenfield, D. Artificial Intelligence in Medicine: Applications, Implications, and Limitations. 2019. Available online: https: //sitn.hms.harvard.edu/flash/2019/artificial-intelligence-in-medicine-applications-implications-and-limitations/ (accessed on 25 May 2021).

13. Amisha.; Malik, P.; Pathania, M.; Rathaur, V. Overview of artificial intelligence in medicine. J. Fam. Med. Prim. Care **2019**, 8, 2328. [CrossRef]

14. Faust, O.; Hagiwara, Y.; Hong, T.J.; Lih, O.S.; Acharya, U.R. Deep learning for healthcare applications based on physiological signals: A review. Comput. Methods Programs Biomed. **2018**, 161, 1–13. [CrossRef]

15. Islam, M.M.; Karray, F.; Alhajj, R.; Zeng, J. A Review on Deep Learning Techniques for the Diagnosis of Novel Coronavirus (COVID-19). IEEE Access **2021**, 9, 30551–30572. [CrossRef]

16. Shi, F.; Wang, J.; Shi, J.; Wu, Z.; Wang, Q.; Tang, Z.; He, K.; Shi, Y.; Shen, D. Review of Artificial Intelligence Techniques in Imaging Data Acquisition, Segmentation, and Diagnosis for COVID-19. IEEE Rev. Biomed. Eng. **2021**, 14, 4–15. [CrossRef] [PubMed]

17. Hemdan, E.E.D.; Shouman, M.A.; Karar, M.E. COVIDX-Net: A Framework of Deep Learning Classifiers to Diagnose COVID-19 in X-Ray Images. arXiv **2020**, arXiv:eess.IV/2003.11055.

18. Khan, A.; Sohail, A.; Zahoora, U.; Qureshi, A.S. A survey of the recent architectures of deep convolutional neural networks. Artif. Intell. Rev. **2020**, 53, 5455–5516. [CrossRef]

19. Sethy, P.K.; Behera, S.K.; Ratha, P.K.; Biswas, P. Detection of coronavirus Disease (COVID-19) based on Deep Features and Support Vector Machine. Int. J. Math. Eng. Manag. Sci. **2020**, 5, 643–651. [CrossRef]

20. Khan, A.I.; Shah, J.L.; Bhat, M.M. CoroNet: A deep neural network for detection and diagnosis of COVID-19 from chest x-ray images. Comput. Methods Programs Biomed. **2020**, 196, 105581. [CrossRef] [PubMed]

21. Rajaraman, S.; Siegelman, J.; Alderson, P.O.; Folio, L.S.; Folio, L.R.; Antani, S.K. Iteratively Pruned Deep Learning Ensembles for COVID-19 Detection in Chest X-Rays. IEEE Access **2020**, 8, 115041–115050. [CrossRef]

22. Chowdhury, M.E.H.; Rahman, T.; Khandakar, A.; Mazhar, R.; Kadir, M.A.; Mahbub, Z.B.; Islam, K.R.; Khan, M.S.; Iqbal, A.; Emadi, N.A.; et al. Can AI Help in Screening Viral and COVID-19 Pneumonia? IEEE Access **2020**, 8, 132665–132676. [CrossRef]

23. Ucar, F.; Korkmaz, D. COVIDiagnosis-Net: Deep Bayes-SqueezeNet based diagnosis of the coronavirus disease 2019 (COVID-19) from X-ray images. Med. Hypotheses **2020**, 140, 109761. [CrossRef]

24. Rahimzadeh, M.; Attar, A. A modified deep convolutional neural network for detecting COVID-19 and pneumonia from chest X-ray images based on the concatenation of Xception and ResNet50V2. Inform. Med. Unlocked **2020**, 19, 100360. [CrossRef]

25. Narin, A.; Kaya, C.; Pamuk, Z. Automatic detection of coronavirus disease (COVID-19) using X-ray images and deep convolutional neural networks. Pattern Anal. Appl. **2021**, 24, 1207–1220. [CrossRef]

26. Khobahi, S.; Agarwal, C.; Soltanalian, M. CoroNet: A Deep Network Architecture for Semi-Supervised Task-Based Identification of COVID-19 from Chest X-ray Images. Available online: https://www.medrxiv.org/content/early/2020/04/17/2020.04.14.2006 5722 (accessed on 25 May 2021).

27. Wang, L.; Lin, Z.Q.; Wong, A. COVID-Net: A tailored deep convolutional neural network design for detection of COVID-19 cases from chest X-ray images. Sci. Rep. **2020**, 10, 19549. [CrossRef]

28. Afshar, P.; Heidarian, S.; Naderkhani, F.; Oikonomou, A.; Plataniotis, K.N.; Mohammadi, A. COVID-CAPS: A capsule networkbased framework for identification of COVID-19 cases from X-ray images. Pattern Recognit. Lett. **2020**, 138, 638–643. [CrossRef]

29. Abbas, A.; Abdelsamea, M.M.; Gaber, M.M. Classification of COVID-19 in chest X-ray images using DeTraC deep convolutional neural network. Appl. Intell. **2020**, 51, 854–864. [CrossRef]

30. Minaee, S.; Kafieh, R.; Sonka, M.; Yazdani, S.; Soufi, G.J. Deep-COVID: Predicting COVID-19 from chest X-ray

images using deep transfer learning. Med. Image Anal. **2020**, 65, 101794. [CrossRef]

31. Punn, N.S.; Agarwal, S. COVID-19 Posteroanterior Chest X-Ray Fused (CPCXR) Dataset. Available online: https://ieee-dataport. org/documents/covid-19-posteroanterior-chest-x-ray-fused-cpcxr-dataset (accessed on 25 May 2021).

32. Cohen, J. COVID-19 Chest X-ray Dataset. Available online: https://github.com/ieee8023/covid-chestxray-dataset (accessed on 25 May 2021).

33. Radiological Society of North America. RSNA Pneumonia Detection Challenge. Available online: https://www.kaggle.com/c/ rsna-pneumonia-detection-challenge (accessed on 25 May 2021).

34. Antani, S. Tuberculosis Chest X-ray Image Data Sets. - LHNCBC Abstract. Available online: https://lhncbc.nlm.nih.gov/LHCpublications/pubs/TuberculosisChestXrayImageDataSets.html (accessed on 25 May 2021).

35. Punn, N.S.; Agarwal, S. Automated diagnosis of COVID-19 with limited posteroanterior chest X-ray images using fine-tuned deep neural networks. Appl. Intel. **2020**, 51, 2689–2702. [CrossRef]

36. Scherer, D.; Müller, A.; Behnke, S. Evaluation of Pooling Operations in Convolutional Architectures for Object Recognition. In Artificial Neural Networks–ICANN 2010; Springer: Berlin/Heidelberg, Germany, 2010; pp. 92–101._10. [CrossRef]

37. Ranzato, M.; Huang, F.J.; Boureau, Y.L.; LeCun, Y. Unsupervised Learning ofw Invariant Feature Hierarchies with Applications to Object Recognition. In Proceedings of the 2007 IEEE Conference on Computer Vision and Pattern Recognition, Minneapolis, MN, USA, 17–22 June 2007; pp. 1–8. [CrossRef]

38. Nwankpa, C.; Ijomah, W.; Gachagan, A.; Marshall, S. Activation Functions: Comparison of trends in Practice and Research for Deep Learning. arXiv **2018**, arXiv:1811.03378.

39. Keras. Keras Documentation: About Keras. Available online: https://keras.io/ (accessed on 25 May 2021).

40. TensorFlow. Available online: https://www.tensorflow.org/ (accessed on 25 May 2021).

41. Brutzkus, A.; Globerson, A. Why do Larger Models Generalize Better? A Theoretical Perspective via the XOR Problem. In Proceedings of the 36th International Conference on Machine Learning(ICML), Long Beach, CA, USA, 9–15 June 2019.

42. Singh, D.; Kumar, V.; Yadav, V.; Kaur, M. Deep Neural Network-Based Screening Model for COVID-19-Infected Patients Using Chest X-Ray Images. Int. J. Pattern Recognit. Artif. Intell. **2020**, 35, 2151004. [CrossRef]

43. Sahinbas, K.; Catak, F.O. Transfer learning-based convolutional neural network for COVID-19 detection with X-ray images. In Data Science for COVID-19; Elsevier: Amsterdam, The Netherlands, 2021; pp. 451–466.

44. Medhi K.; Jamil, M.; Hussain, I. Automatic Detection of COVID-19 Infection from Chest X-ray Using Deep Learning. Available online: https://www.medrxiv.org/content/10.1101/2020.05.10.20097063v1 (accessed on 25 May 2021).

45. Maguolo, G.; Nanni, L. A Critic Evaluation of Methods for COVID-19 Automatic Detection from X-ray Images. arXiv **2020**, arXiv:eess.IV/2004.12823.